PHYSICAL REVIEW D **79,** 061101(R) (2009)

New limits on spin-independent and spin-dependent couplings of low-mass WIMP dark matter with a germanium detector at a threshold of 220 eV

S. T. Lin,[1] H. B. Li,[1] X. Li,[2] S. K. Lin,[1] H. T. Wong,[1,*] M. Deniz,[1,3] B. B. Fang,[2] D. He,[2] J. Li,[2,4] C. W. Lin,[1] F. K. Lin,[1] X. C. Ruan,[5] V. Singh,[1,6] A. K. Soma,[1,6] J. J. Wang,[1] Y. R. Wang,[1] S. C. Wu,[1] Q. Yue,[2] and Z. Y. Zhou[5]

(TEXONO Collaboration)

[1]*Institute of Physics, Academia Sinica, Taipei 115, Taiwan*
[2]*Department of Engineering Physics, Tsinghua University, Beijing 100084, China*
[3]*Department of Physics, Middle East Technical University, Ankara 06531, Turkey*
[4]*Institute of High Energy Physics, Chinese Academy of Science, Beijing 100039, China*
[5]*Department of Nuclear Physics, Institute of Atomic Energy, Beijing 102413, China*
[6]*Department of Physics, Banaras Hindu University, Varanasi 221005, India*

(Received 10 December 2007; revised manuscript received 22 May 2008; published 12 March 2009)

An energy threshold of (220 ± 10) eV was achieved at an efficiency of 50% with a four-channel ultralow-energy germanium detector, each with an active mass of 5 g. This provides a unique probe to weakly interacting massive particles (WIMP) dark matter with mass below 10 GeV. With a data acquisition live time of 0.338 kg-day at the Kuo-Sheng Laboratory, constraints on WIMPs in the galactic halo were derived. The limits improve over previous results on both spin-independent WIMP-nucleon and spin-dependent WIMP-neutron cross-sections for WIMP mass between 3 and 6 GeV. Sensitivities for full-scale experiments are projected. This detector technique makes the unexplored sub-keV energy window accessible for new neutrino and dark matter experiments.

DOI: 10.1103/PhysRevD.79.061101 PACS numbers: 95.35.+d, 95.55.Vj, 95.85.Ry, 98.35.Gi

There is compelling evidence from cosmological and astrophysical observations that about one quarter of the energy density of the universe can be attributed to cold dark matter (CDM), whose nature and properties are still unknown [1]. Weakly interacting massive particles (WIMP, denoted by χ) are the leading candidates for CDM. There are intense experimental efforts [2] to look for WIMPs through direct detection of nuclear recoils in $\chi N \rightarrow \chi N$ elastic scattering or in the studies of the possible products through $\chi\bar{\chi}$ annihilations. Supersymmetric (SUSY) particles [3] are the leading WIMP candidates. The popular SUSY models prefer WIMP mass (m_χ) in the range of $\sim$100 GeV, though light neutralinos remain a possibility [4]. Most experimental programs optimize their design in the high-mass region and exhibit diminishing sensitivities for $m_\chi < 10$ GeV, where an allowed region due to the annual modulation data of the DAMA experiment [5]—further reinforced by the first DAMA/LIBRA results [6]—remains unprobed. Simple extensions of the standard model with a singlet scalar favor light WIMPs [7]. Detectors with a sub-keV threshold are required to probe this low-mass region, as well as WIMPs bounded in the solar system [8] and nonpointlike SUSY candidates like Q-balls [9]. This presents a formidable challenge to both detector technology and background control. Only the CRESST-I experiment has set limits [10] with a sapphire (Al_2O_3)-based cryogenic detector at a threshold of 600 eV.

The Kuo-Sheng (KS) Laboratory [11] is located at 28 m from a reactor core at 2.9 GW thermal power. The overburden is about 30 m-water-equivalence. A threshold of 5 keV and a background level of $\sim$1 event kg^{-1} keV^{-1} day^{-1} (cpkkd) at 20 keV, comparable with those of underground CDM experiments, were achieved on a 1.06-kg germanium detector (HPGe). Results on neutrino magnetic moments (μ_ν) [12], reactor electron neutrinos [13], and reactor axions [14] were reported. The current goal is to develop detectors with kg-scale target mass, 100 eV-range threshold and low-background specifications for the studies of WIMPs, μ_ν, and neutrino-nucleus coherent scatterings [15].

The ultralow-energy germanium detector (ULEGe) is a matured technology for sub-keV soft x-rays measurements. These detectors typically have a modular mass of 5–10 g, while detector arrays of up to 30 elements have been constructed. Compared with Al_2O_3, Ge provides enhancement in χN spin-independent couplings ($\sigma^{\rm SI}_{\chi N}$) due to the A^2 dependence [1,16], where A is the mass number of the target isotopes. The isotope ^{73}Ge (natural isotopic abundance of 7.73%) comprises an unpaired neutron such that it can provide an additional probe to the spin-dependent couplings of WIMPs with the neutrons ($\sigma^{\rm SD}_{\chi n}$). The nuclear recoils from χN interactions in the ULEGe only give rise to $\sim$20% of the observable ionizations compared with electron recoils at the same energy. The suppression ratio is called the quenching factor (QF) [17].

*Corresponding author.
FAX:+886-2-2788-9828.
htwong@phys.sinica.edu.tw;

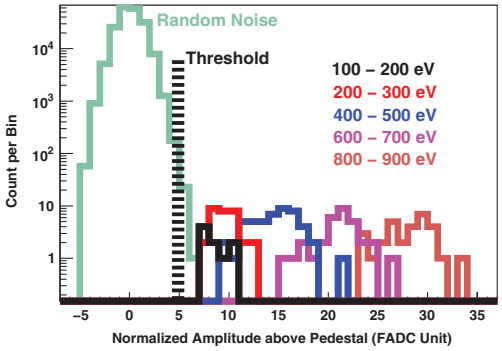

FIG. 1 (color). The distributions of noise fluctuation of RT events and the maximum amplitudes of physics events in various energy bins. The discriminator threshold level is also shown.

For clarity, all ULEGe measurements discussed hereafter are electron-equivalent-energy, unless otherwise stated.

The ULEGe array consists of four elements, each having an active mass of 5 g [18]. Standard ultralow-background specifications were adopted in its construction and choice of materials. It has identical external dimensions as the 1 kg HPGe of Ref. [12]. Apart from swapping between the two detectors, data taking was performed with all other hardware components, shielding configurations, electronics, and data acquisition (DAQ) systems [19] kept identical. The schematic diagram of the experimental setup can be referred to those displayed in Ref. [12].

The ULEGe signals were provided by built-in pulsed optical feedback preamplifiers and were distributed to two spectroscopy amplifiers at 6 μs(SA_6) and 12 μs(SA_{12}) shaping times and with different amplification factors. The SA_6, SA_{12}, anti-Compton veto (ACV), and cosmic-ray veto (CRV) signals were read out by 20 MHz flash analog-to-digital convertors (FADC). Random trigger (RT) events at 0.1 Hz and uncorrelated with the rest of the system, as well as various system control parameters, were also recorded. The discriminator output of SA_6 provided the trigger for DAQ. As depicted in Fig. 1, the threshold was set to about 4.3 ± 0.2 times the rms fluctuations of the RT signals above the pedestal. The DAQ rates for the ULEGe were about 5 Hz, induced mostly by electronic noise and agreed well with expectations [20,21].

Energy measurements were given by SA_{12}^T, defined in the next paragraph. Figure 2(a) shows an energy calibration spectrum with external ^{55}Fe sources (5.90 and 6.49 keV) together with x rays from Ti (4.51 and 4.93 keV), Ca (3.69 keV), and S (2.31 keV). Photons with energy lower than 2 keV were completely absorbed by the detector window. The RT events provided the calibration point at zero energy. The rms resolutions for the RT events and ^{55}Fe peaks were about 55 eV and 78 eV, respectively. The calibration procedures were performed before and after the DAQ periods. Linearity was checked up to 60 keV with various γ sources, and between zero and 2 keV with a precision pulse generator. The energy scale was accurate to $<$20 eV, while deviations from linearity were $<$1%. The

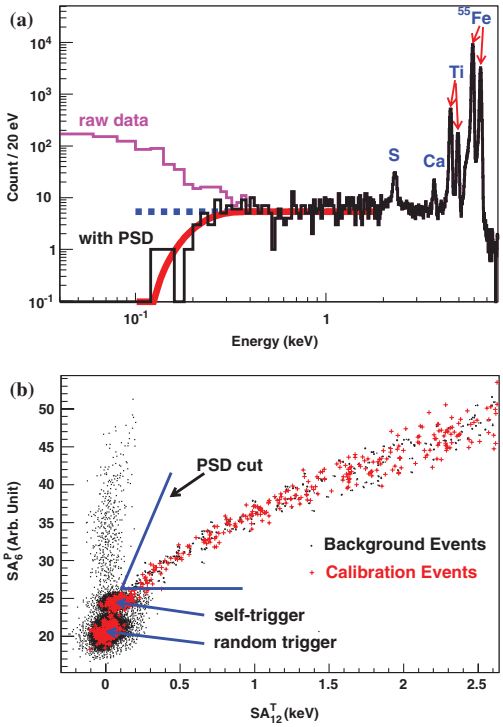

FIG. 2 (color). (a) Measured energy spectrum of the ULEGe with ^{55}Fe source together with x-ray peaks from various materials. The black histogram represents events selected by PSD cuts. Deviations from the expected flat spectra contribute to PSD efficiencies. (b) Scatter plots of the SA_6^P vs SA_{12}^T signals, for both calibration and physics events. The PSD selection is shown.

electronic gain drifts, also monitored *in situ* by the pulse generator, were $<$5%. A detector hardware "noise edge" of about 300 eV was achieved.

Pulse shape discrimination (PSD) software was devised to differentiate physics events from those induced by electronic noise, exploiting the correlations in both the energy and timing information of SA_6 and SA_{12} signals. Displayed in Fig. 2(b) is a scatter plot of SA_6^P and SA_{12}^T signals with the PSD cut superimposed, where the superscripts P/T denote partial/total integration of the pulses within $(15, 25)$ μs and $(-20, 52)$ μs, respectively, relative to the

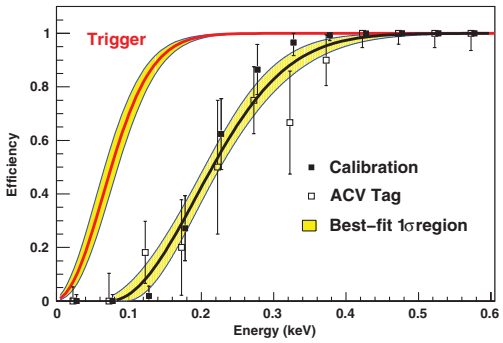

FIG. 3 (color). Selection efficiencies of the PSD cut, as derived from the ^{55}Fe calibration and *in situ* data with ACV tags. Also shown are the best-fit 1σ region and the trigger efficiency for physics events recorded by the DAQ system.

TABLE I. Summary of analysis results and their statistical and systematic errors in the two energy intervals which define the sensitivities at low and high WIMP masses.

Energy bin	198–241 eV	1.39–1.87 keV
Raw background counts	105212	75
Selection cuts and systematic effects :		
Trigger efficiency (%)	100	
DAQ dead time (%)	11.0 ± 0.1	
PSD—cumulative background survival fraction (%)	0.008	97
Signal efficiency (%)	66 ± 6	100
ACV—cumulative background survival fraction (%)	0.0	2.7
Signal efficiency (%)	98.3 ± 0.1	
CRV—cumulative background survival fraction (%)	0.0	0.0
Signal efficiency (%)	91.4 ± 0.1	
After-cut background counts	0	0
After-cut normalized background rates ($\mathrm{kg}^{-1}\,\mathrm{keV}^{-1}\,\mathrm{day}^{-1}$)	$0 \pm {}^{272}_{0}\,(\mathrm{stat}) \pm {}^{30}_{27}\,(\mathrm{sys})$	$0 \pm {}^{13}_{0}\,(\mathrm{stat}) \pm 0(\mathrm{sys})$
Quenching factor	0.200 ± 0.006	0.244 ± 0.007
Sampling in m_χ (GeV)	5	50
$\sigma^{\mathrm{SI}}_{\chi N}(10^{-39}\ \mathrm{cm}^2)$:		
Mean and errors due to background and QF uncertainties	$0 \pm {}^{0.64}_{0}\,(\mathrm{Bkg}) \pm 0.01(\mathrm{QF})$	$0 \pm {}^{0.153}_{0}\,(\mathrm{Bkg}) \pm 0.003(\mathrm{QF})$
Limit at 90% confidence level	<0.81	<0.20
$\sigma^{\mathrm{SD}}_{\chi n}(10^{-34}\ \mathrm{cm}^2)$:		
Mean and errors due to background and QF uncertainties	$0 \pm {}^{1.90}_{0}\,(\mathrm{Bkg}) \pm 0.03(\mathrm{QF})$	$0 \pm {}^{0.47}_{0}\,(\mathrm{Bkg}) \pm 0.01(\mathrm{QF})$
Limit at 90% confidence level	<2.40	<0.59

trigger instant ($t = 0$). The noise events were suppressed. Calibration events and those from a physics background were overlaid, indicating a uniform response. Events selected by PSD but with CRV or ACV tags were subsequently rejected. The surviving events were ULEGe signals uncorrelated with other detector systems and could be WIMP candidates.

Data were taken with the ULEGe at KS with different hardware and software configurations. They provided important input on the background understanding and performance optimizations for future full-scale experiments. The data set with the best background and threshold has a DAQ live time of 0.338 kg-day. The analysis results and the systematic effects at the two energy intervals which defined the sensitivities for m_χ below and above $\sim$10 GeV are summarized in Table I.

The ULEGe data were taken in conjunction with a CsI (Tl) scintillator array [22] for the studies of neutrino-electron scattering. The combined DAQ rate was about 30 Hz. The DAQ dead time and the CRV + ACV selection efficiencies listed in Table I were accurately measured using RT events [12]. The maximum amplitude distributions of the physics events between 100 eV and 900 eV are shown in Fig. 1. All events exhibit at least 1 FADC-unit of margin above the threshold. The mean and rms of the samples above 300 eV were directly derived from the data, while those for $E = 0$–300 eV were evaluated by interpolation to avoid biased sampling. The pedestal was provided by the RT events. The trigger efficiencies depicted in Fig. 3 correspond to the fractions of the distributions above the discriminator threshold level.

Events in coincidence with ACV are mostly physics-induced. Displayed in Fig. 4 is the survival fraction (f) of ACV-tagged events at $E = 200$–300 eV in PSD selection vs the relative timing between ACV signals and ULEGe triggers. The coincidence interval between the two systems was determined independently from hardware timing. *Only* ULEGe events in coincidence with ACV give a substantial value of f. Events without ACV tags are predominantly induced by electronic noise. They were efficiently rejected by the PSD selection. The corresponding $f_N = (1.7 \pm 0.3) \times 10^{-4}$ is denoted by the data point at negative time in Fig. 4. The PSD efficiency for physics

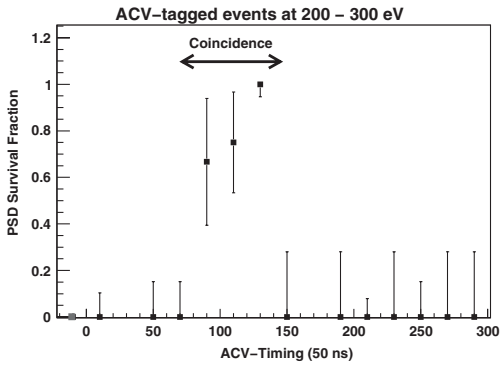

FIG. 4. The survival fraction of events at $E = 200$–300 eV with ACV tags in PSD selection vs the relative timing between ACV signals and ULEGe triggers. Overlaid are the coincidence time intervals derived independently from hardware timing. The data point at negative time is due to events without ACV tags, and corresponds to $(1.7 \pm 0.3) \times 10^{-4}$.

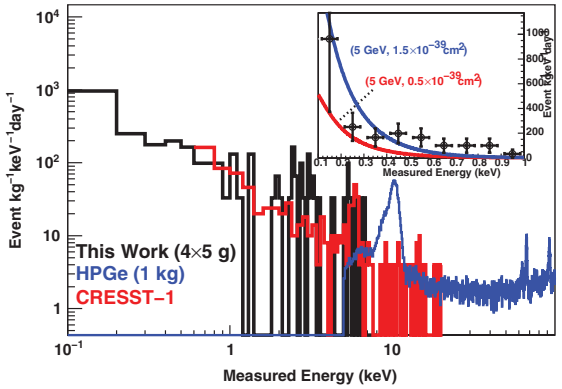

FIG. 5 (color). The measured spectrum of ULEGe with 0.338 kg-day of data, after CRV, ACV, and PSD selections. Background spectra of the CRESST-I experiment [10] and the HPGe [12] are overlaid for comparison. The expected nuclear recoil spectra for two cases of $(m_\chi, \sigma^{\rm SI}_{\chi N})$ are superimposed onto the spectrum shown in linear scales in the inset.

events ($\epsilon_{\rm PSD}$) is

$$f = \frac{(\epsilon_{\rm PSD} * P + f_N * N)}{P + N},$$

where P and N are, respectively, the fractions of physics and noise events in the ACV-tagged samples. In general, there are noise events in accidental coincidence with ACV (that is, $N > 0$), which implies $\epsilon_{\rm PSD} \geq f$. The conservative assignment of taking $\epsilon_{\rm PSD} = f$ (equivalently $N = 0$) was adopted for analysis.

Alternatively, under the assumption that the ^{55}Fe calibration of Fig. 2(a) would give rise to physics events with a flat spectrum down to the lowest energy relevant to this analysis (< 100 eV), the deviations of the PSD-selected events from a flat distribution provided the second measurement. Consistent results were obtained with both approaches, as depicted in Fig. 3. The larger uncertainties of the first method are attributed to the limited statistics from only the *in situ* ACV samples. The efficiencies and their uncertainties adopted for analysis were derived from a best fit on the combined data set. A threshold of (220 ± 10) eV was achieved with a PSD efficiency of 50%.

The ULEGe spectrum normalized in cpkkd unit after the CRV, ACV, and PSD selections is displayed in Fig. 5, showing comparable background as CRESST-I [10]. Listed in Table I are the normalized background rates, indicating that statistical uncertainties dominate over the systematic effects. The formalisms followed those of Ref. [16], using standard nuclear form factors, a galactic rotational velocity of 230 km s^{-1}, and a local WIMP density of 0.3 GeV cm^{-3} with Maxwellian velocity distribution. No subtraction of background profiles was made such that the WIMP signals cannot be larger than the observed event rates. The unbinned optimal interval method formulated in Ref. [23] and widely used by current CDM experiments was adopted to derive the upper limits for the possible χN event rates. By comparing the observed background in different energy intervals with the expected number of events due to χN recoils for each m_χ, the optimal intervals producing the most stringent limits to $\sigma^{\rm SI}_{\chi N}$ and $\sigma^{\rm SD}_{\chi n}$ were selected. Corrections from QF, detector resolution, and various efficiency factors were incorporated. The energy dependence of QF in Ge was evaluated with the TRIM software package [24] which matches existing data [25] better than the alternative Lindhard model [26]. The uncertainties were taken to be the difference with the polynomial best-fit values of the data from 254 eV to 200 keV nuclear recoil energy.

Exclusion plots on both $(m_\chi, \sigma^{\rm SI}_{\chi N})$ and $(m_\chi, \sigma^{\rm SD}_{\chi n})$ planes at 90% confidence level for galactically-bound WIMPs were then derived, as depicted in Figs. 6(a) and 6(b),

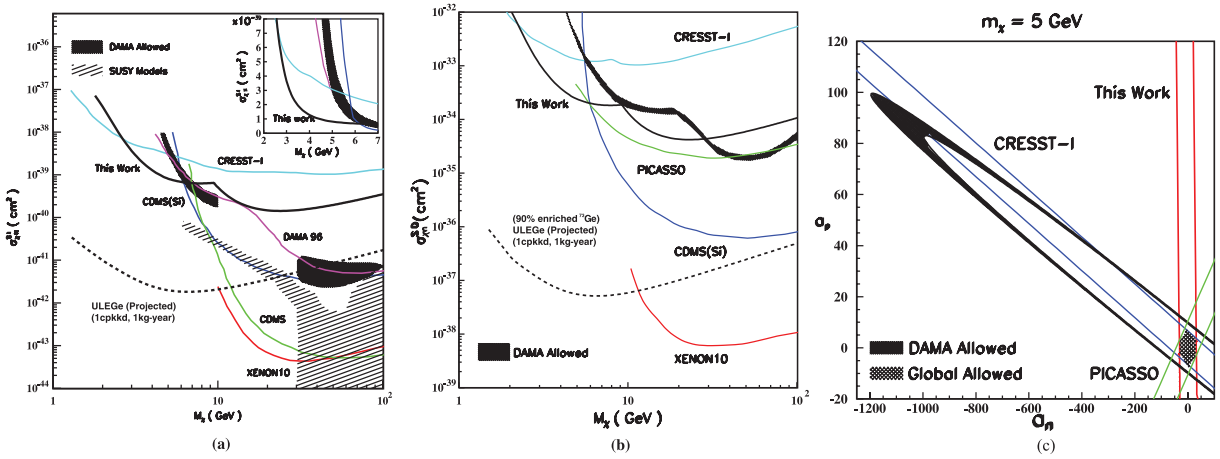

FIG. 6 (color). Exclusion plots of (a) the spin-independent χN and (b) the spin-dependent χ-neutron cross-sections versus WIMP mass, displaying the KS-ULEGe limits and those defining the current boundaries [10,27]. The DAMA-allowed regions [5] are superimposed. The striped regions are those favored by SUSY models [4]. Projected sensitivities of full-scale experiments are indicated as dotted lines. (c) Constraints at $m_\chi = 5$ GeV on the effective axial four-fermion χ-proton (a_p) and χ-neutron (a_n) spin-dependent couplings, in units of $2\sqrt{2}G_{\rm F}$ following the formulation of Ref. [29]. The shaded area at the origin is the combined allowed region.

respectively. The DAMA-allowed regions [5] and the current exclusion boundaries [10,27] are displayed. The model-independent approach of Refs. [28,29] were adopted to extract limits on the spin-dependent cross sections. Consistent results were obtained when different ^{73}Ge nuclear physics matrix elements [30] were adopted as input. The constraints on the effective axial four-fermion χ-proton and χ-neutron spin-dependent couplings [29] at $m_\chi = 5$ GeV are displayed in Fig. 6(c). The parameter space probed by the ^{73}Ge in ULEGe is complementary to that of the CRESST-I experiment [10] where the ^{27}Al target is made up of an unpaired proton instead. New limits were set by the KS-ULEGe data in both $\sigma^{\mathrm{SI}}_{\chi N}$ and $\sigma^{\mathrm{SD}}_{\chi n}$ for $m_\chi \sim 3$–6 GeV. The remaining DAMA low-m_χ allowed regions in both interactions were probed and excluded. The observable nuclear recoils at $m_\chi = 5$ GeV and $\sigma^{\mathrm{SI}}_{\chi N} = 0.5 \times 10^{-39}$ cm^2 (allowed) and 1.5×10^{-39} cm^2 (excluded) are superimposed with the measured spectrum in the inset of Fig. 5 for illustrations. It is expected that recent data from the COUPP [31] experiment can place further constraints on the spin-dependent plots of Figs. 6(b) and 6(c).

This work extends the bounds on WIMPs by making measurements in a new observable window of 100 eV–1 keV in a low-background environment. Understanding and suppression of background at this sub-keV region is crucial for further improvement. Measurements are conducted with the ULEGe at an underground laboratory. There are recent advances in a ''point-contact'' Ge detector [32] which offer potentials of scaling up the detector mass to the kg range. Preliminary results in dark matter searches have recently been reported [33]. The mass-normalized external background will be reduced in massive detectors because of self-attenuation [15]. A further reduction in threshold may be possible with improved junction field-effect transistors and by correlating signals from both electrodes. The potential reach of full-scale experiments with 1 kg-year of data and a benchmark background level of 1 cpkkd is illustrated in Figs. 6(a) and 6(b). Such experimental programs are complementary to the many current efforts on CDM direct searches.

We are grateful to the KIMS Collaboration and the authors of Ref. [20] for inspiring comments. This work is supported by the Academia Sinica Pilot Project 2004–06, Theme Project 2008–10, Contracts No. 95-2119-M-001-028 and No. 96-2119-M-001-005 from the National Science Council, Taiwan, and Contract No. 10620140100 from the National Natural Science Foundation, China.

[1] M. Drees and G. Gerbier, J. Phys. G **33**, 233 (2006), and references therein.
[2] R. J. Gaitskell, Annu. Rev. Nucl. Part. Sci. **54**, 315 (2004), and references therein.
[3] H. H. Haber and M. Schmitt, J. Phys. G **33**, 1105 (2006).
[4] A. Bottino *et al.*, Phys. Rev. D **72**, 083521 (2005), and references therein.
[5] C. Savage, P. Gondolo, and K. Freese, Phys. Rev. D **70**, 123513 (2004); P. Gondolo and G. Gelmini, Phys. Rev. D **71**, 123520 (2005); R. Bernabei *et al.*, Riv. Nuovo Cimento Soc. Ital. Fis. **26N1**, 1 (2003).
[6] R. Bernabei *et al.*, Eur. Phys. J. C **56**, 333 (2008).
[7] X. G. He *et al.*, Mod. Phys. Lett. A **22**, 2121 (2007).
[8] T. Damour and L. M. Krauss, Phys. Rev. Lett. **81**, 5726 (1998); J. I. Collar, Phys. Rev. D **59**, 063514 (1999).
[9] G. Gelmini, A. Kusenko, and S. Nussinov, Phys. Rev. Lett. **89**, 101302 (2002).
[10] G. Angloher *et al.*, Astropart. Phys. **18**, 43 (2002).
[11] H. T. Wong, Mod. Phys. Lett. A **19**, 1207 (2004).
[12] H. T. Wong and H. B. Li, Mod. Phys. Lett. A **20**, 1103 (2005); H. B. Li *et al.*, Phys. Rev. Lett. **90**, 131802 (2003); H. T. Wong *et al.*, Phys. Rev. D **75**, 012001 (2007).
[13] B. Xin *et al.*, Phys. Rev. D **72**, 012006 (2005).
[14] H. M. Chang *et al.*, Phys. Rev. D **75**, 052004 (2007).
[15] H. T. Wong *et al.*, J. Phys. Conf. Ser. **39**, 266 (2006).
[16] J. D. Lewin and P. F. Smith, Astropart. Phys. **6**, 87 (1996).
[17] J. F. Ziegler, J. P. Biersack, and U. Littmark, *The Stopping and Range of Ions in Solid* (Pergamon Press, New York, 1985).
[18] Manufacturer: Canberra Industries, Inc.
[19] W. P. Lai *et al.*, Nucl. Instrum. Methods Phys. Res., Sect. A **465**, 550 (2001).
[20] F. T. Avignone III, P. S. Barbeau, and J. I. Collar, arXiv:0806.1314.
[21] P. J. Statham, X-Ray Spectrom. **6**, 94 (1977).
[22] H. B. Li *et al.*, Nucl. Instrum. Methods Phys. Res., Sect. A **459**, 93 (2001).
[23] S. Yellin, Phys. Rev. D **66**, 032005 (2002).
[24] J. F. Ziegler, Transport of Ions in Matter, http://www.srim.org (1998).
[25] K. W. Jones and H. W. Kraner, Phys. Rev. C **4**, 125 (1971); Phys. Rev. A **11**, 1347 (1975); T. Shutt *et al.*, Phys. Rev. Lett. **69**, 3425 (1992); Y. Messous *et al.*, Astropart. Phys. **3**, 361 (1995).
[26] J. Lindhard *et al.*, Mat. Fys. Medd. K. Dan. Vidensk. Selsk. **33**, 10 (1963).
[27] R. Bernabei *et al.*, Phys. Lett. B **389**, 757 (1996); M. Barnabe-Heider *et al.*, Phys. Lett. B **624**, 186 (2005); J. Angle *et al.*, Phys. Rev. Lett. **100**, 021303 (2008); Z. Ahmed *et al.* (CDMS Collaboration), Phys. Rev. Lett. **102**, 011301 (2009).
[28] A. Bottino *et al.*, Phys. Lett. B **402**, 113 (1997).
[29] D. R. Tovey *et al.*, Phys. Lett. B **488**, 17 (2000).
[30] M. T. Ressell *et al.*, Phys. Rev. D **48**, 5519 (1993); V. I. Dimitrov, J. Engel, and S. Pittel, Phys. Rev. D **51**, R291 (1995).
[31] E. Behnke *et al.*, Science **319**, 933 (2008).
[32] P. A. Barbeau, J. I. Collar, and O. Tench, J. Cosmol. Astropart. Phys. 09 (2007) 009.
[33] C. E. Aalseth *et al.*, arXiv:0807.0879.